Check for updates

Received: 22 August 2021 | Revised: 19 December 2021 | Accepted: 19 December 2021

DOI: 10.1111/gcb.16064

Global Change Biology WILEY

RESEARCH ARTICLE

Remote sensing of cytotype and its consequences for canopy damage in quaking aspen

Benjamin Blonder[1,2,3] | Philip G. Brodrick[4] | James A. Walton[5] | Katherine Dana Chadwick[6,7] | Ian K. Breckheimer[2] | Suzanne Marchetti[8] | Courtenay A. Ray[1,2,3] | Karen E. Mock[5]

[1]Department of Environmental Science, Policy, and Management, University of California, Berkeley, Berkeley, California, USA

[2]Rocky Mountain Biological Laboratory, Crested Butte, Colorado, USA

[3]School of Life Sciences, Arizona State University, Tempe, Arizona, USA

[4]Jet Propulsion Laboratory, California Institute of Technology, Pasadena, California, USA

[5]Department of Wildland Resources, Utah State University, Logan, Utah, USA

[6]Department of Earth System Science, Stanford University, Stanford, California, USA

[7]Climate and Ecosystems Division, Lawrence Berkeley National Laboratory, Berkeley, California, USA

[8]Forest Health Protection, United States Forest Service, Gunnison, Colorado, USA

Correspondence
Benjamin Blonder, 54 Mulford Hall, Department of Environmental Science, Policy, and Management, UC Berkeley, Berkeley, CA 94720, USA.
Email: benjamin.blonder@berkeley.edu

Funding information
Department of Energy; Microsoft AI 4 Earth; National Science Foundation, Grant/Award Number: DBI-1755522 and EAR-1725788; Arizona State University; Jet Propulsion Laboratory; California Institute of Technology; National Aeronautics and Space Administration

Abstract

Mapping geographic mosaics of genetic variation and their consequences via genotype x environment interactions at large extents and high resolution has been limited by the scalability of DNA sequencing. Here, we address this challenge for cytotype (chromosome copy number) variation in quaking aspen, a drought-impacted foundation tree species. We integrate airborne imaging spectroscopy data with ground-based DNA sequencing data and canopy damage data in 391 km^2 of southwestern Colorado. We show that (1) aspen cover and cytotype can be remotely sensed at 1 m spatial resolution, (2) the geographic mosaic of cytotypes is heterogeneous and interdigitated, (3) triploids have higher leaf nitrogen, canopy water content, and carbon isotope shifts ($\delta^{13}C$) than diploids, and (4) canopy damage varies among cytotypes and depends on interactions with topography, canopy height, and trait variables. Triploids are at higher risk in hotter and drier conditions.

KEYWORDS
aspen, cytotype, forest mortality, genotype × environment interaction, G×E, hyperspectral, imaging spectroscopy, landscape genetics, ploidy level, remote sensing

1 | INTRODUCTION

Large extent, high-resolution maps of intraspecific genetic variation could provide information for forecasting species range shifts in response to climate change (Parmesan & Yohe, 2003). However, maps of species distributions based on environmental data (Elith & Leathwick, 2009) rarely account for genetic variability beyond the species level. This is because spatially mapping intraspecific genetic variation (Fitzpatrick & Keller, 2015) is challenging and resource-intensive, requiring detailed field sampling

Benjamin Blonder, Philip G. Brodrick, James A. Walton and K. D. Chadwick contributed equally.

 © 2022 John Wiley & Sons Ltd.

followed by intensive DNA-based analyses. Remote sensing has the potential to unveil geographic mosaics of genetic variation at greater extents and resolution than previously considered. Such maps would enable investigating genotype × environment interactions (G×E) at the landscape scale, enabling studies of G×E to reach beyond the laboratory and greenhouse into natural populations.

Mapping genetic variation and assessing its impact on range shifts could be resolved through the development of methods that infer genetic information from high spectral resolution imagery. Genetic variation that modifies leaf chemistry (e.g., water content or pigments) or structure (e.g., canopy structure) modifies the light reflected by the canopy (Asner, 1998; Asner et al., 2017; Clark et al., 2005; Curran, 1989). Canopy reflectance has been used to detect shifts in foliar chemistry (Chadwick & Asner, 2016; Martin et al., 2018; Singh et al., 2015), and to discriminate species (Baldeck et al., 2015; Ferreira et al., 2016; Fricker et al., 2019). Similar approaches potentially could infer intraspecific genetic variation. Leaf reflectance spectra have recently been used to identify population structure and hybrids in *Dryas* spp. (Stasinski et al., 2021). Additionally, recent studies have used drones or aircraft-based hyperspectral imagery to identify genetic variation (Blonder, Graae, et al., 2020; Czyż et al., 2020) or genetic boundaries (Madritch et al., 2014) in tree species, but have been limited to smaller mapping applications.

A key component of genetic variation is cytotype, the number of copies of each chromosome, also known as 'ploidy level' (Levin, 1983; Stebbins, 1971). Cytotype variation is common within many plant species, including crops, rangeland grasses, and trees (Keeler, 1998; Petit et al., 1999). Individuals with triploid cytotypes may have phenotypes associated with the more resource acquisitive end of the plant economics spectrum (Díaz et al., 2016), supporting more rapid growth in high-resource environments but also increased vulnerability to drought and pathogens in these conditions (a G×E effect affecting mortality). A key potential mechanism is an increase in genome size which drives increases in cell size (Roddy et al., 2020). For xylem, this could drive a greater risk of embolism (Sperry et al., 2008) and for stomata and mesophyll cells, this could drive shifts in water use efficiency and photosynthesis (Roddy et al., 2020; Théroux-Rancourt et al., 2021). A second key mechanism is the higher gene expression in polyploids, which could also drive increased pathogen risk due to the re-allocation of resources toward growth instead of defense (Kruger et al., 2020).

Quaking aspen (*Populus tremuloides* Michx.) is a model system for understanding landscape variation in intraspecific cytotype variation and its interaction with the environment. Aspen is a broadleaf and foundation tree species with a range spanning from Alaska to Mexico (DeByle & Winokur, 1985; Mitton & Grant, 1996). Mortality of aspen forests has been observed since the early 2000s in the southwestern part of the species' range (Worrall et al., 2013).

Aspen has diploid and triploid cytotypes (Einspahr et al., 1963; Every & Wiens, 1971). Cytotypes can co-occur within a region (Mock et al., 2008), and triploidy may be more common in the Southwest (Mock et al., 2012), which is also where drought mortality has been highest (Dixon & DeWald, 2015; Worrall et al., 2013). Triploids are thought to have traits that confer taller and faster growth (Benson & Einspahr, 1967; Every & Wiens, 1971; Flansburg, 2018) and to have more resource-acquisitive leaves (Greer et al., 2017).

Topography also creates a spatial mosaic of environmental variation, which is also likely to be important for mortality. Drought is often a major contributor to decline, with mortality occurring 3–5 years after onset due to accumulation of hydraulic damage in stems (Anderegg et al., 2013), and exacerbated by fire or disease (Marchetti et al., 2011; Rogers et al., 2014). Mortality has primarily been observed on south-facing aspects, at lower elevations, and for taller/older canopies (Worrall et al., 2008, 2013), strongly suggestive of a role for heat and drought. Hydraulic ecophysiology models support this perspective (Anderegg et al., 2015; Tai et al., 2017) as do sap flow data (Liu & Biondi, 2021) and conceptual expectations (Adams et al., 2017; Martinez-Vilalta et al., 2019). However, the role of G×E interactions on canopy damage and mortality—that is, differential responses of diploids and triploids—remains to be explored.

Here, we ask: (1) Can airborne spectroscopy successfully classify aspen cytotype?; (2) What are the drivers and patterns of aspen cytotype at the landscape scale?; (3) How do canopy traits vary with cytotype and other factors; and (4) How does canopy damage vary with cytotype, canopy traits, canopy height, and topography? We address these questions using airborne imaging spectroscopy, field-measured genomic data, and aerial and LiDAR survey data at 110 m resolution and 391 km^2 extent over Colorado (Figure 1a; Figure S1). The main advance of this study is in mapping genetic features and exploring G×E interactions at the large spatial extent and high resolution, relative to prior studies in aspen that have mapped genetic features at either smaller extents (Blonder, Graae, et al., 2020) or have focused on delineating genotype boundaries rather than genetic feature per se (Madritch et al., 2014). Our central and previously untested hypothesis is that G×E interactions cause triploid aspen to be at greater risk for canopy damage in hotter and drier environments.

2 | MATERIALS AND METHODS

2.1 | Study area

The study was carried out over 391 km^2 of land area near Crested Butte, Colorado (Figure 1a; Figure S1). The landscape comprises glacially carved valleys and mountains, covered by meadows, aspen forest, conifer forest, tundra, and ranchland. Elevations range from 2678 to 4104 m. Spatial analyses were carried out at 1 m resolution on WGS84/UTM-13N projection within R (version 4.0.3) using the *terra* and *sf* packages.

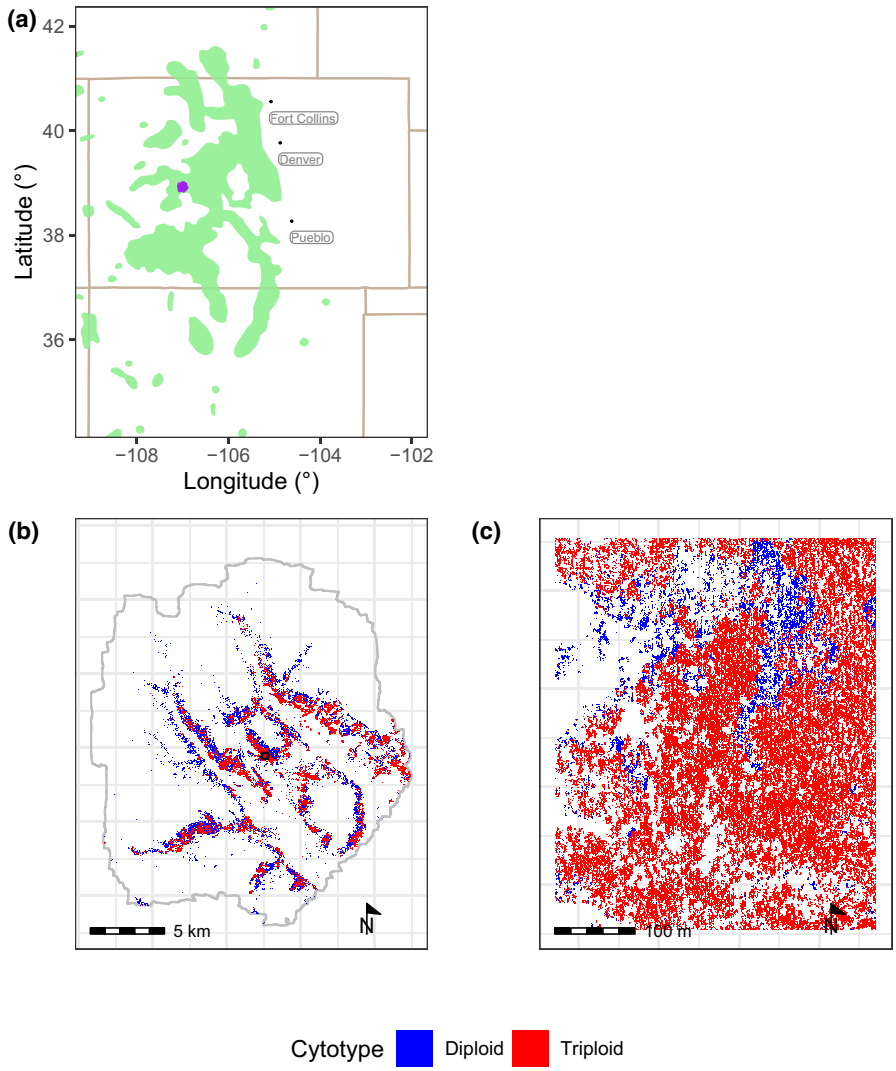


FIGURE 1 (a) The study region is shown in purple within a map of Colorado. Green polygon indicates the range of quaking aspen according to Little (1971). (b) Map of aspen distribution and cytotype distribution within the study region predicted from hyperspectral imagery. Diploids are shown in blue; triploids in red. (c) Inset corresponding to the rectangular region in (b)

2.2 | Hyperspectral, LiDAR, and canopy height data

We obtained hyperspectral reflectance data to use directly for cytotype mapping (Q1, Q2), trait mapping (Q3), and damage analyses (Q4). In June 2018, the study area was overflown by the National Ecological Observatory Network (NEON) Airborne Observation Platform (AOP), via Twin Otter aircraft (Chadwick, Brodrick, Grant, Goulden, et al., 2020). Flights were timed for when the majority of vegetation had leafed out, and occurred over two weeks during mid-morning sunny conditions, at approximately 1000 m above ground level. Data were collected by a pushbroom imaging spectrometer (NASA Jet Propulsion Laboratory).

We also obtained Lidar data that was used directly to generate a canopy height predictor for use in Q2, Q3, and Q4 analyses, as well as several intermediate variables. Waveform LiDAR (Optech ALTM Gemini) was collected simultaneously with reflectance data (Goulden & Musinsky, 2020). Spectroscopy data were converted from at-sensor radiance to surface reflectance through an iterative, localized version of the ACORN atmospheric correction package (Brodrick et al., 2020; Chadwick & Brodrick, 2020). LiDAR data were processed to surface elevation, canopy height, and shade (Goulden et al., 2020).

2.3 | Trait data

We mapped aspen canopy functional traits for Q3 and as potential predictors of canopy damage in Q4. Traits were chosen as proxies for several axes of strategy variation, respectively, variation in water storage and canopy closure, water use efficiency, and photosynthetic capacity. NEON imaging spectroscopy data were used to generate maps of canopy water content (ml m^{-2}), leaf carbon isotope shift ($\delta^{13}C$; per mil relative to Pee Dee Belemnite standard), and leaf nitrogen (%) across the study extent. Trait mapping was carried out by training machine learning models (ensembles of partial least squares regression models) on the reflectance data and a large number of field measurements of each trait across vegetation types. Approximately 400 field samples were collected from sunlit leaves of meadow, shrub, and tree vegetation types within three days of the NEON AOP overflight. Samples were dried and then run on an elemental analyzer coupled to a mass spectrometer for C and

N concentrations and $\delta^{13}C$ (Chadwick, Grant, et al., 2020). Canopy water content was physically retrieved from spectral data. Mean trait predictions and estimated error rates were obtained from model ensembles. Full details of field data and statistical methods are published in (Chadwick, Brodrick, Grant, Henderson, et al., 2020) and summarized at https://kdchadwick.github.io/east_river_trait_modeling/. We removed pixels where the standard deviation of prediction between models exceeded 0.8‰ for $\delta^{13}C$ and 0.15% for nitrogen, and clipped values to canopy water content above 0 ml m^{-2}; leaf carbon isotope shift between −30 and −22‰; and nitrogen between 0% and 15%.

2.4 | Genetic data

We also generated a range of georeferenced genomic data for use in training models of cytotype underlying Q1–Q4 analyses. In summer 2018, we established 503 plots distributed throughout the study area within the aspen cover (Figure S2; Blonder et al., 2021; Blonder, Walton, et al., 2020). Thirty-nine percent of plots were randomly located, 55% were located in four rectangular grids (one per watershed, with 25 m spacing between plots), and 6% were opportunistically located in areas of high canopy damage or habitat types undersampled by the random plots (e.g., talus, tundra). Plots were constrained to non-wilderness public land and trust land. Each plot was centered at a focal living tree and identified by installing an aluminum tag. The location of the focal tree was determined using a GPS unit (Trimble, Geo 7X, <1 m horizontal accuracy with point averaging). To further refine coordinates to sub-meter accuracy, we also re-visited a subset of 280 plots in 2019, using the RGB orthomosaic data loaded onto a handheld tablet with a GPS unit (Garmin GLO2), then manually delineated crown polygons for focal trees based on local spatial context. Polygon centroids were used as final coordinates for these plots.

2.5 | DNA-based cytotype data

We used a slingshot and line technique (Youngentob et al., 2016) to obtain canopy branches of each focal tree in summer 2018. A healthy mature leaf was selected and preserved in silica desiccant at room temperature. DNA was extracted from leaf tissue using a Qiagen DNeasy plant kit, and double-digest restriction fragment-based DNA libraries were prepared using a method similar to that described by (Gompert et al., 2012). Libraries were sequenced in three lanes at the University of Texas Genomic Sequencing and Analysis Facility on an Illumina HiSeq2500 for single-end 100bp reads. Samples were then classified for clonal membership using the pairwise distribution of Jaccard similarities (Rowe, 2019) and classified for cytotype (diploid or triploid) using algorithms described by (Gompert & Mock, 2017), yielding 480/503 successful classifications. A total of 191 clones (genotypes) are represented in this dataset. Detailed methods are available in (Blonder et al., 2021) and RADseq data are available at (Blonder, Walton, et al., 2020).

2.6 | Canopy damage data

We obtained canopy damage data as a response variable for Q4 analyses. We defined canopy damage as any vegetative damage leading to temporary or permanent defoliation and/or aboveground stem loss, from any source. Longer-term responses (resprouting or complete stem/root mortality) could also occur, so this variable does not necessarily indicate whole-plant mortality, although it could. Canopy damage was assessed via two complementary approaches.

First, we used rasterized Aerial Detection Survey data for 2000–2018 from the US Forest Service (Coleman et al., 2018). We selected polygons comprising any mapped damage (branch dieback or canopy loss). Our selection criteria differ slightly from (Worrall et al., 2013) by including additional years of data and damage from all sources rather than only putative drought mortality. This more liberal criterion includes damage from sources like an insect or fungal pathogens whose ultimate cause may be drought (Marchetti et al., 2011). The majority of aspen damage in this region (Figure S3) has occurred (to date) in the mid-2000s (Worrall et al., 2013). This dataset has broad spatial and temporal coverage and includes all types of damage events. It is limited by relatively coarse spatial resolution (~100 m) and by aggregation of 2000–2018 damage relative to 2018 traits and cytotypes. As such, it cannot distinguish cases in which prior canopy damage was sustained or recovered, nor can it distinguish whether prior canopy mortality led to replacement by a stand of the same or different cytotype.

Second, we used repeated airborne LiDAR surveys to identify locations where canopy height decreased by large amounts. A first overflight of the study extent was carried out on August 10, 2015 by Quantum Spatial with a Riegl(Leica) Q1560 discrete-return LiDAR system on a Piper Navajo aircraft. This acquisition yielded a point cloud with a density of 14.4 points m^{-2} (Wainwright & Williams, 2017). A second overflight was carried out from August 21 to September 24, 2019 using a Riegl(Leica) VQ1560i system mounted on a Cessna Caravan aircraft, resulting in a point cloud with a density of 9.4 points m^{-2} (Breckheimer, 2021). Both scans met the USGS QL2 quality standard (Heidemann, 2018; Table S1). Ground-classified returns in each tile were triangulated to create a bare-earth surface, and this elevation was subtracted from the point cloud elevations. Canopy heights were estimated using a pit-free model of the canopy surface (Khosravipour et al., 2014). Canopy heights were differenced, gridded at 1/3 m resolution, and median-aggregated to 1-m resolution. Areas of avalanches and landslides were manually masked, and the remaining dataset was further masked to aspen cover. Canopy damage was inferred for pixels in which canopy height decreased between 2015 and 2019 by >3 m. This dataset has a higher spatial resolution and a shorter temporal extent than the USFS data, enabling clearer linkages to 2018 cytotype and trait data. It is limited by a reduced spatial extent (151 km^2) and its inclusion of only canopy damage that led to decreases in canopy height. Defoliation and canopy damage that does not lead to treefall are not captured.

In both cases, these damage metrics also are associated with ground-based measurements of stem mortality (Figure 2). We

measured stem mortality in all plots in 2018 by checking cambium greenness (Blonder et al., 2021). Fractions of numbers of dead stems per plot are higher in plots whose location falls in pixels indicated as damaged in both the 2015–2018 Lidar data, as well as in the 2015–2018 subset of the USFS data.

2.7 | Aspen and cytotype classification (Q1)

Two independent models were trained to: (1) separate out land cover type, and (2) distinguish between cytotypes. For (1), we hand-delineated 465 polygons that corresponded to aspen forests occurring in a range of topographic positions, and in all of the watersheds. We also hand-delineated 1168 polygons with similar areas, which were selected to be in other land cover types (built environment, conifer, dry meadow, mesic meadow, miscellaneous bare ground, snow, water, and woody riparian vegetation). We extracted spectral reflectance data at all wavelengths for all pixels, then brightness-normalized and scaled values (excluding dominant atmospheric water absorption features during brightness normalization). These data were then used to train an artificial neural network (ANN) classifier in Python. Parameter grid searches were compared using validation datasets to select a final model structure. The selected model had six layers, 200 nodes, a dropout rate of 0.4 between each layer, and a leaky-ReLU loss function with an alpha of 0.3, similar to previously used species classifiers (Chadwick, Brodrick, Grant, Henderson, et al., 2020). The response function (surface class) was weighted to account for class imbalance, with sample weight proportional to the inverse of the total class count. The model was trained with an Adam optimizer for 10 epochs. Cover maps were converted to a binary indicator of aspen cover throughout the study area and used as a mask for below remote sensing analyses.

For (2), training data were obtained by extracting brightness-normalized reflectance data in a 5 m × 5 m square grid around each ground-based plot for which cytotype data were available, excluding non-aspen pixels (using the cover map described above), as well as shade-masked pixels (n = 50,294 buffered pixels). We then assumed that all of these data represented pixels of the same cytotype as the focal tree because our gridded ground-based datasets indicate that cytotype variation occurs at 25–50 m spatial scales in this region (Blonder et al., 2021). Using this training data set, parameter grid searches were used to select a model with five internal layers of 200 nodes, a dropout rate of 0.5, batch normalization between each layer, and a softplus activation function (with a sigmoid activation function after the last layer). Weighting was used for class imbalance, and the model was trained for 32 epochs with an Adam optimizer using an initial learning rate of 0.0005 until the test set precision and recall rates peaked. We predicted both models on the full hyperspectral image dataset, and in the case of the cytotype model, masking out shaded and non-aspen classified pixels. Cytotype predictions were sieved using a 20 px minimum size requirement. Next, a temporary prediction was made by passing a median filter over the predictions using a 10 m spatial kernel. The median filtered values were then used to fill in the sieve-caught pixels. This sieving and filtering helped identify rare unrealistic cases where one cytotype was surrounded entirely by another. This processed dataset was then used for all downstream analyses. Figure S2 shows predictions overlaid with plot data.

2.8 | Random forest modeling approach (Q2–Q4)

We fit several random forest models using a common approach using the *ranger* package. Random forest algorithms were used because of their good performance and generalization, as well as low computational cost. We first mean-aggregated all data products to 10 m resolution, ignoring missing values, to reduce model degradation from noisy pixels. Binary variables (aspen cover, cytotype, canopy damage) were converted to within-pixel fractions. Aggregated pixel values for all datasets were extracted, and subsetted only to pixels that were at least 50% aspen, eliminating isolated 1 m pixels (n = 91,051 remaining 10 m pixels).

Random forest model response variables comprised diploid cytotype fraction (Q2), traits (Q3), or canopy damage fraction (Q4). Predictor variables comprised topographic features (Q2–Q4), canopy height (Q2–Q4), diploid cytotype fraction (Q3, Q4), and/or traits (Q4). Models were fit using 1000 trees and a maximum tree depth of 10. A k-fold spatially explicit cross-validation was carried out, balancing prevalence of response variables for categorical responses, then dividing data into 100 × 100 m patches, then training models on one randomly selected subset of patches (80%), and testing model performance on another randomly selected subset (20%).

Performance was evaluated on test subsets in terms of R^2. To determine which variables contributed to performance, models were fit using all subsets of predictor types (cytotypes, traits, canopy height, and/or topography).

Partial dependence plots (PDPs) were used to show the mean predicted response for the entire dataset, when individual features are fixed at different values, and demonstrate how the model, on average, utilized changes in features. That is, PDPs indicate the direct and independent effect of a predictor on the response. PDPs were generated for each replicate model and then visualized as ensemble means and coefficients of variation (mean/SD) using the *pdp* package.

2.8.1 | Cytotype spatial patterning (Q2)

Models used 2018 cytotype as response and all subsets of topographic variables and/or canopy height as predictors.

2.8.2 | Trait analysis (Q3)

Models used each 2018 trait variable as a response, and included all subsets of 2018 cytotype, canopy height, and/or topographic predictors.

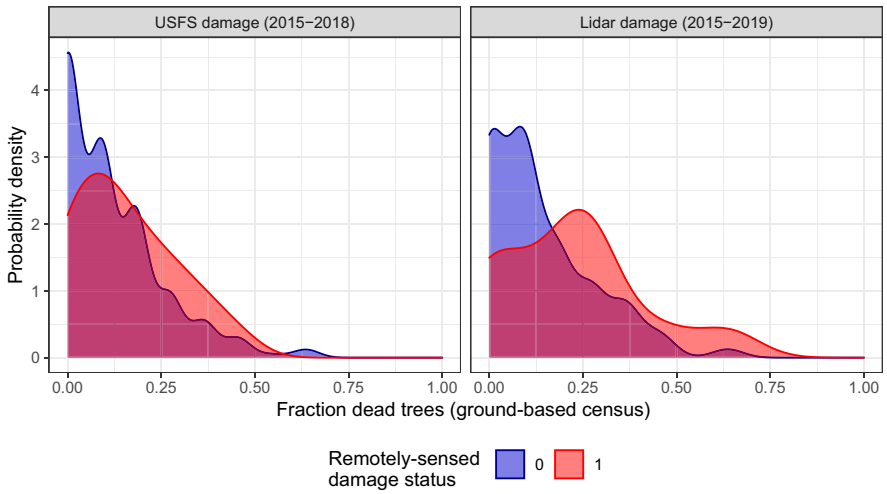


FIGURE 2 Comparison of remotely sensed canopy damage metrics relative to ground-based mortality surveys. The *y*-axis here indicates dead tree fractions in each of 503 aspen plots from Blonder et al. (2021; from which the genetic data from this study are also sourced). Density plots indicate that canopy damage, as determined either from the USFS or Lidar data, is higher in plots with more dead trees

2.8.3 | Canopy damage analysis (Q4)

Models used canopy damage fraction as a response, for each of the 2000–2018 USFS and all subsets of 2015–2019 LiDAR datasets, and 2018 cytotype, canopy height, topography, and/or 2018 traits as predictors.

3 | RESULTS

3.1 | Question 1—Mapping cytotypes

Aspen cover and aspen cytotype were classifiable with high success from the hyperspectral imagery. Spectral variation among aspen-classified pixels also was evident among diploids and triploids, especially at around 600, 950, 1250, 1700, and 2200 nm (Figure S4a). The classifier for aspen versus non-aspen cover achieved a specificity (true negative rate) in a spatially explicit hold-out test set of 99.9% and a sensitivity (true positive rate) of 97.3% (Figure S4c). The classifier for cytotype achieved 86.9% specificity and 83.6% sensitivity in a spatially explicit hold-out test set (Figure S4e).

3.2 | Question 2—Cytotype spatial patterning

Diploid and triploid cytotypes occurred across the landscape in complex patterns that were often homogeneous but sometimes showed interdigitation (Figure 1b,c; Figure S3). Of the 12.8 km^2 area classified as aspen within the study extent, triploid pixels were more common than diploid pixels (57.5% vs. 42.5%; Figure S5).

Diploid fractions increased at high elevation and high values of cosine aspect (north-facing slopes), with the converse true for triploids (Figure 3; Figure S6; R^2 = .18 ± 0.005 SD). The overall prevalence of observed aspen points had a unimodal distribution centered at intermediate elevation and canopy water content values (Figure S7).

3.3 | Question 3—Trait analysis

Canopy water content (CWC) varied from approximately 2200 to 3000 ml m^{-2} in aspen (Figure 4a). Triploids had higher CWC than diploids. Overall, CWC was lower in shorter canopies and on south-facing slopes (lower cosine aspect; Figure 5a; Figure S8a; R^2 = .43 ± 0.016 SD).

Leaf carbon isotope shift ($\delta^{13}C$) varied from approximately −25.8 to −25.0 per mil in aspen (Figure 4b). Triploids had higher $\delta^{13}C$ than diploids. Overall, $\delta^{13}C$ was higher with greater canopy height and combinations of greater canopy height and north-facing aspect (Figure 5b; Figure S8b; R^2 = .38 ± 0.0010 SD).

Leaf nitrogen (N) varied from approximately 2.2%–3.0% in aspen (Figure 4c). Triploids had higher N than diploids. Overall, N was higher on more south-facing aspects and in shorter canopies (Figure 5c; Figure S8c; R^2 = .23 ± 0.016 SD).

The overall pixel prevalence of diploids and triploids grouped by these predictors was highest along an axis spanning from low elevation and north aspect to mid-elevation and south aspect, and was similar among diploids and triploids (Figure S9).

3.4 | Question 4—Canopy damage analysis

Using the 2000–2018 USFS dataset, a total of 2,990,734 of 12,829,327 m^2 of the unshaded aspen-classified area experienced canopy damage (23.3%). Among healthy pixels, 54% were triploid, whereas among pixels with canopy damage, 68% were triploid (Figure S10a). Maximum canopy damage fraction was higher for triploids, especially at intermediate elevations (R^2 = 0.13 ± 0.014 SD). In

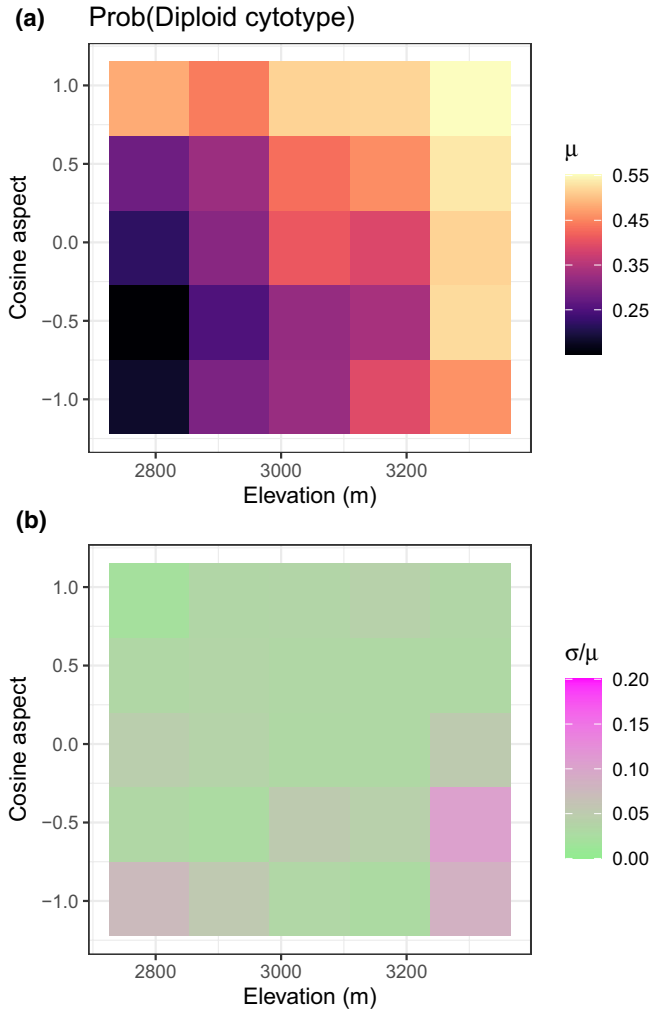


FIGURE 3 (a) Partial dependence plot of cytotype (probability of diploid vs triploid) on elevation and cosine aspect, as mean (μ) prediction of a model ensemble based on topography and canopy height predictors. Negative values indicate south-facing slopes while positive values indicate north-facing slopes. (b) Coefficient of variation (standard deviation, σ, divided by μ) of ensemble predictions

contrast, diploid canopy damage fraction was higher at higher elevations (though this conclusion is more tentative due to the higher coefficient of variation in predictions at this predictor combination). There was no strong effect of canopy water content on canopy damage fraction (Figure 6a; Figure S11a). These results were consistent when the models were fit on the more restricted extent of the LiDAR data below (Figures S11c and S12).

In contrast, using the 2015–2019 LiDAR dataset, a total of 90,285 of 6,694,627 m^2 (1.3%) of the unshaded aspen-classified area was classified as canopy damage. Among healthy pixels, 61% were triploid, whereas among pixels with canopy damage, 56% were triploid (Figure S10b). In triploids, canopy damage fraction was higher at low elevation and low canopy water content, while in diploids, canopy damage fraction was higher at low elevation regardless of canopy water content (Figure 6b; Figure S11b; $R^2 = .03 \pm 0.006$ SD).

The overall prevalence of diploids and triploids grouped by these predictors was highest at intermediate elevation and low canopy water content for diploids, and at intermediate elevation and intermediate canopy water content for triploids (Figure S13).

4 | DISCUSSION

This study was able to map previously hidden landscape genetic patterns through the integration of DNA and remote sensing datasets. The genetic maps also suggest that aspen, triploids, and diploids experience different canopy damage rates, as determined by interactions with topography and canopy traits. Thus, these results support the hypothesis of G×E interactions at the landscape scale and provide partial support for the hypothesis of higher canopy damage for triploids in hot and dry environments.

4.1 | Mapping cytotype (Question 1)

Aspen cytotypes were mappable at high resolution and a large extent using imaging spectroscopy data, underscoring the utility of remote sensing in complementing ground-based genomic sampling. The large regions of homogeneous cytotypes in the predicted maps are consistent with expectations of extensive clonal growth in western North America (DeWoody et al., 2008; Mock et al., 2008). The use of a pixel-based classification algorithm with spatially-explicit test sets also builds confidence in these predictions.

4.2 | Spatial variation in cytotype (Question 2)

These genetic maps illuminate the spatial distribution of cytotypes within a large heterogeneous landscape, consistent with observations of landscape heterogeneity in Colorado aspen phenotypes (Morgan, 1969). Triploid pixels were more common at low elevations and on south-facing slopes, consistent with recent ground-based surveys (Blonder, Graae, et al., 2020; Blonder et al., 2021; Mock et al., 2012). This pattern is indicative of higher performance in hotter and drier environments, confirming drivers that have been long hypothesized (Every & Wiens, 1971) to explain the elevational zonation of different aspen types (Baker, 1921).

Prior landscape disturbance, in addition to topography, could have contributed to these spatial patterns, if demographic responses are cytotype-dependent. Glacial retreat and recolonization dynamics, regular disturbances from avalanches and landslides, and surficial geology may also have had major impacts on aspen cytotype distribution (Blonder et al., 2021). Native American use of the land may have led to further disturbances, e.g., burning and game management in some locations (Kay, 2000).

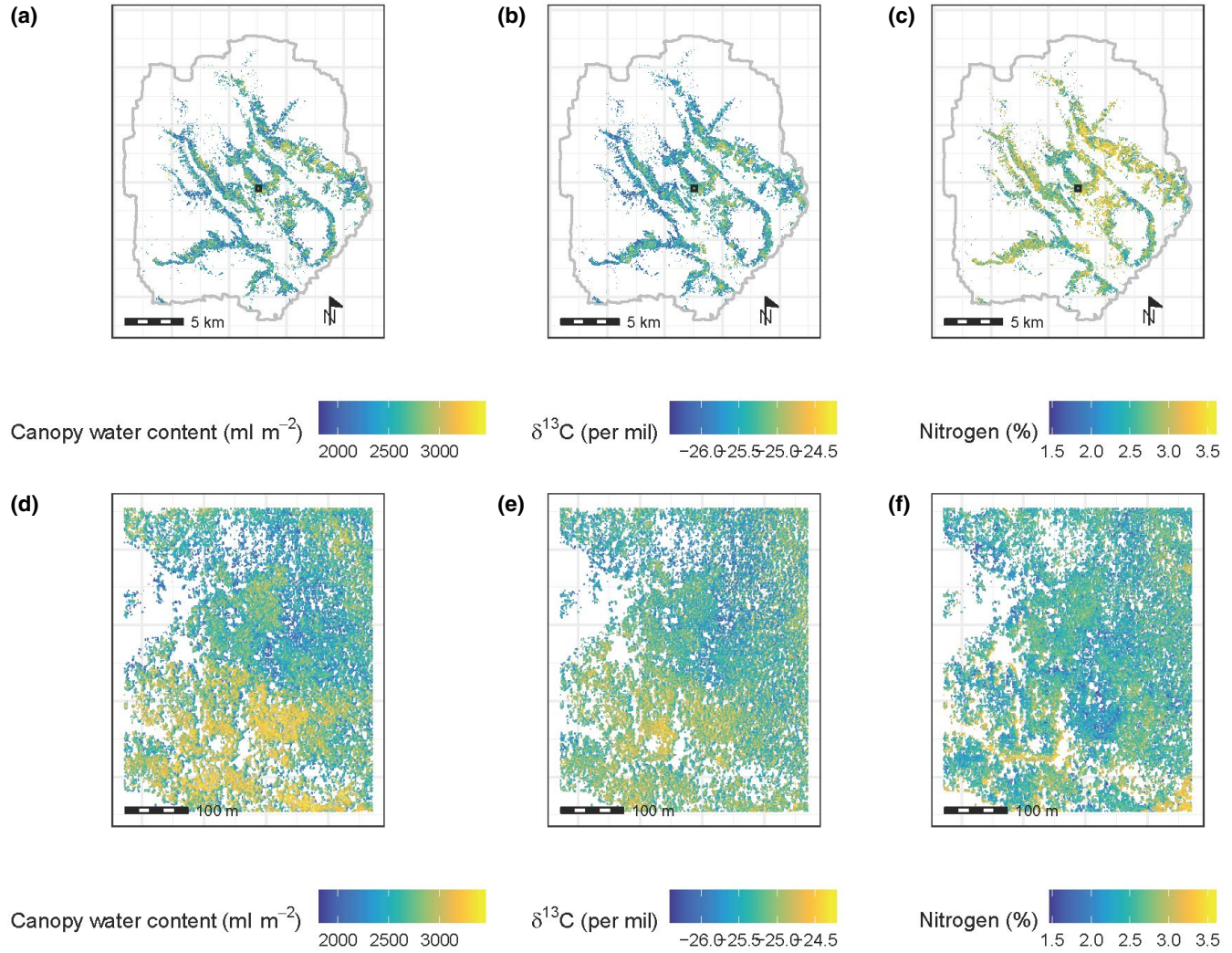


FIGURE 4 Maps of canopy trait distributions inferred for aspen-classified pixels. (a, d) Canopy water content (ml m^{-2}), (b, e) carbon isotope shift, $\delta^{13}C$ (per mil), and (c, f) nitrogen content (%). Panels (d–f) show inset corresponding to the rectangular region in (a–c)

Colonial settlers are also likely to have widespread impacts on land use, most likely in a flatter and more accessible locations (DeByle & Winokur, 1985).

4.3 | Trait predictors (Question 3)

We mapped canopy traits that were associated with cytotype variation, and that provide proxies for potential physiological drivers of cytotype-dependent canopy damage. Triploids had higher canopy water content, which is consistent with greater plant hydration (Martinez-Vilalta et al., 2019) or a higher leaf area index. Triploids also had higher $\delta^{13}C$, consistent with higher water use efficiency. Last, triploids had higher leaf nitrogen, consistent with higher photosynthetic capacity. Nitrogen is not used for secondary defense in aspen (Lindroth & Clair, 2013), but is used to support photosynthesis. These traits are consistent with a "fast-and-risky" strategy for triploids. They also are consistent with patterns reported in a prior ground-based study of trait variation with cytotype in aspen (Greer et al., 2017), and demonstrate that these findings consistently scale up across large landscapes.

Canopy height had a strong effect on all traits beyond the direct effect of topography and cytotype. This effect is consistent with phenotypic differentiation with stand age (assuming height and age are correlated; Donaldson et al., 2006). Thus, canopy traits are likely mediated by successional processes as well as by environmental stressors.

However, our remotely sensed trait data are not able to directly assess the hydraulic traits (e.g., xylem conduit and pit size distributions) or allocation traits (non-structural carbohydrate allocation) that may be more causally linked with drought mortality. In aspen, mortality often lags drought by several years (Anderegg et al., 2013; Brodrick et al., 2019; Goulden & Bales, 2019). Reduced hydraulic capacity resulting from xylem damage could lead to reduced photosynthetic capacity relative to respiration costs in future years, ultimately leading to carbon starvation unless sufficient carbon is available to rebuild hydraulic capacity (Trugman et al., 2018). If triploids have either the higher risk of xylem damage (due to larger sizes

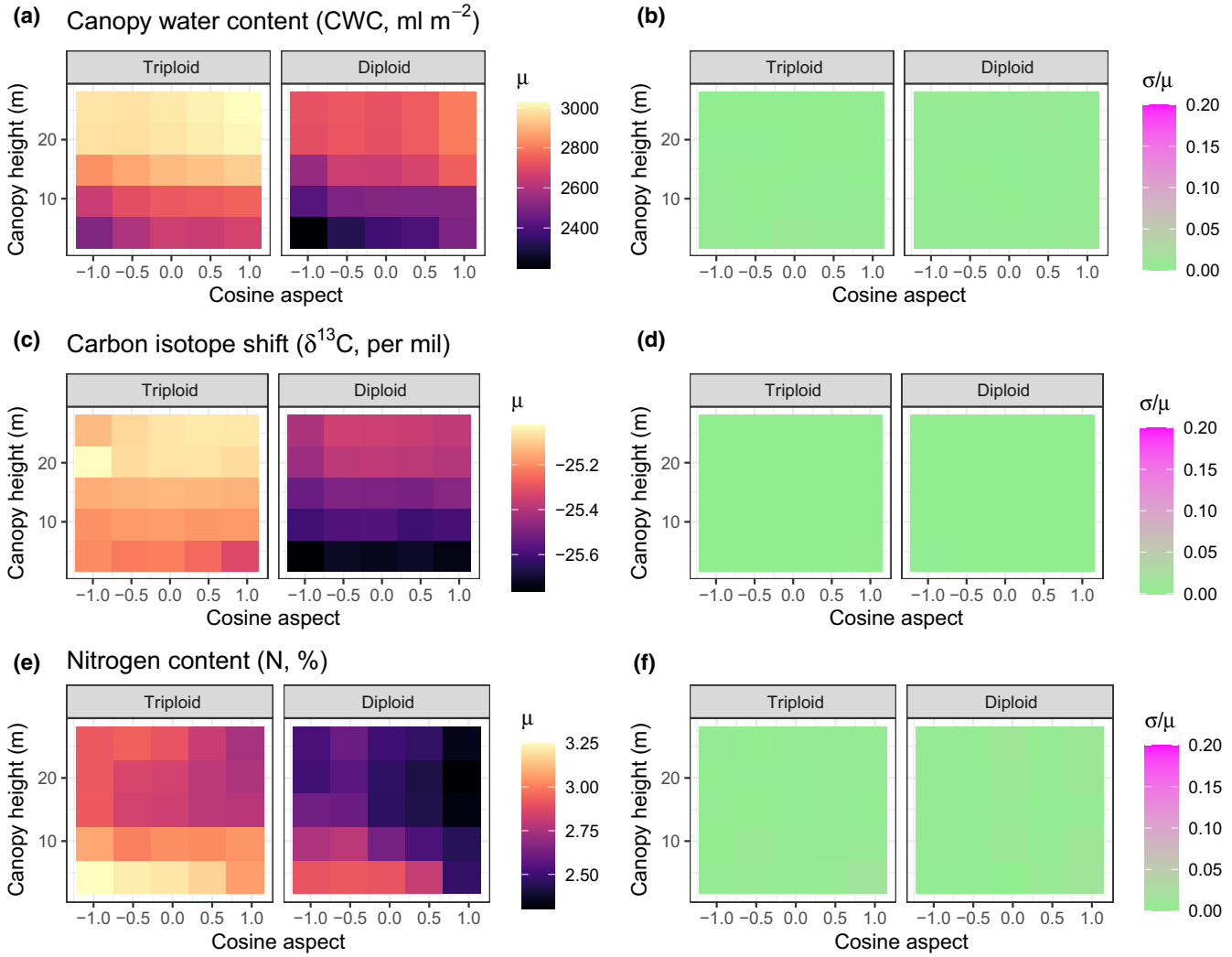


FIGURE 5 Partial dependence plots for each of three traits: (a) canopy water content (ml m^{-2}), (c) leaf carbon isotope shift, δ^{13}C (per mil), and (e) nitrogen content (%), on elevation and cosine aspect, as mean prediction of a model ensemble based on cytotype, canopy height, and topography predictors. (b, d, f) Coefficient of variation (standard deviation, σ, divided by μ) of ensemble predictions

that support rapid growth and more embolism risk) or higher respiration costs or lower non-structural carbohydrate storage (more stem and leaf tissues to support) then these trait patterns would be consistent with this mortality mechanism.

4.4 | Impacts on canopy damage (Question 4)

The effect of cytotype on canopy damage occurred both through direct and interactive effects. However, the spatially cross-validated R^2 was moderate for the USFS analysis and low for the LiDAR analysis, suggesting that the interactive effects of topography, cytotype, traits, and canopy height provided only a partial explanation for the geographic mosaic of canopy damage in the study. Other unmeasured predictors may have also been relevant. Notably, we were not able to include spatiotemporal maps of insect outbreaks or fungal pathogens, which are often important stressors in this species. Our topographic variables also provided an incomplete proxy for environmental variation. For example, we were not able to include detailed spatiotemporal maps of root-zone soil moisture, which likely is key for mediating ecophysiological responses. Making high-resolution gridded predictions of soil moisture remains challenging (Tran et al., 2020).

Several interpretations of the USFS canopy damage results are possible. One interpretation is that past canopy damage primarily affected triploids. Most of the canopy damage in the USFS data comes from the late 2000s, following a ~3–5 year lag following sustained mid-2000s drought (Worrall et al., 2008; Figure S3). This interpretation is consistent either with a higher canopy damage risk for triploids or with the prior landscape containing a greater prevalence of triploids. The interpretation is also consistent with demography results from ground-based surveys (Blonder et al., 2021; Dixon & DeWald, 2015). This interpretation is also consistent with later refoliation and/or regeneration of stems from the rootstock of the same cytotype, as canopy damage does not necessarily indicate whole-plant mortality. Clonal regrowth from suckers is common (DeByle & Winokur, 1985). Such an effect might obscure the main patterns found in this study.

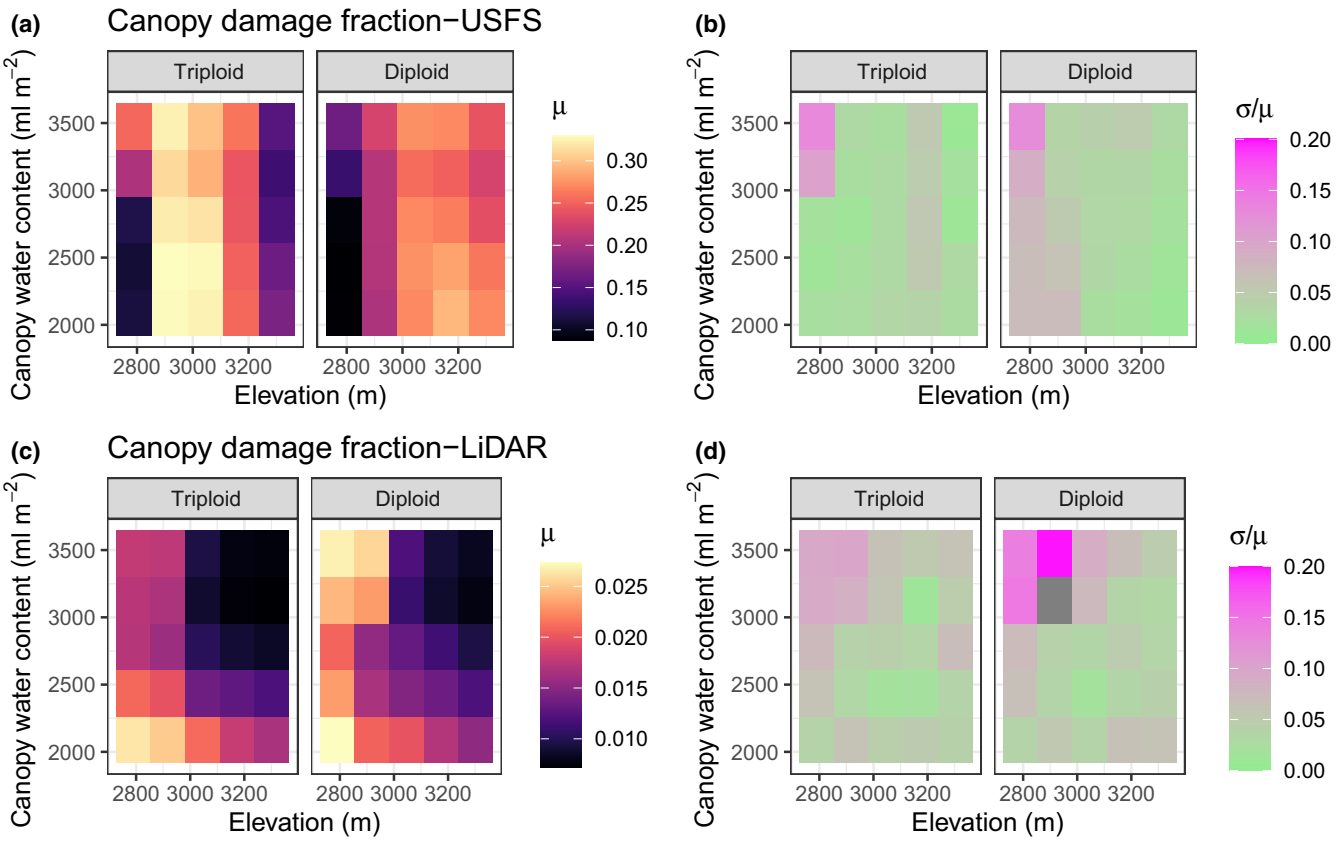


FIGURE 6 Partial dependence plots for canopy damage fraction in (a) 2000–2018 according to USFS aerial survey or (c) 2015–2019 LiDAR treefall data, as mean prediction of a model ensemble based on cytotype, canopy height, topography, and trait predictors. (b, d) Coefficient of variation (standard deviation, σ, divided by μ) of ensemble predictions

An alternate interpretation is that canopy damage primarily affected diploids, which were subsequently replaced by triploids by the time the remote sensing data were collected. We are not able to rule out this possibility as we do not have multiple years of cytotype data available for this landscape, though future work upscaling remote sensing to satellite imagery archives might ultimately resolve this question, as could work using changes in canopy water content or other spectral indices as more spatially resolved proxies of damage and mortality (Brodrick & Asner, 2017; Goulden & Bales, 2019). This is because canopy mortality is thought to be associated with decreases in canopy water content over time (Brodrick & Asner, 2017; Martinez-Vilalta et al., 2019).

The LiDAR data have a closer temporal match to the predictor data. However, the performance of the LiDAR-based canopy damage model was poor, limiting the interpretation of these results. The low overall rates of canopy damage from 2015 to 2019 also suggest that most of the observed patterns may be natural stand turnover, more reflective of the outcomes of cohort aging or succession (Rogers et al., 2014), or of fungal pathogens (Marchetti et al., 2011). The 2015–2019 period also saw high drought (NOAA, 2019), but this may have been too recent to drive canopy damage in the LiDAR data (Anderegg et al., 2013). Canopy damage that did occur may not yet have led to treefall, as dead stems often remain standing for years. We only examined pixels that were classified as an aspen in 2018, minimizing the influence of prior treefall on analyses. However, treefall detected in this interval may be an outcome of mortality occurring several years prior—an effect our data cannot address. Last, the aerial surveys recorded canopy damage at the stand scale across the entire ~400 km^2 domain, and the LiDAR data recorded canopy damage to individual tree crowns in a subset of the study area (151 km^2) that was covered by both LiDAR scans. These mismatches in spatial extents could cause apparent differences in the drivers of damage (Bell et al., 2015). However, we repeated the USFS analysis clipped to the LiDAR data extent and found the main conclusions were not qualitatively different.

While the remotely sensed damage metrics used here are not the same as whole-plant mortality, they were strongly associated with ground-based surveys of aboveground mortality. Thus, we speculate that the prevalence of triploids on the landscape is driven by their greater performance during less extreme climates of the prior centuries and that their dominance may now be challenged by a shift to more extreme climates. Under the assumption that this interpretation is correct, we predict that under future droughts, there will be an overall contraction of aspen ranges in hotter and drier conditions, and that this contraction will disproportionately impact triploids, which tend to be more spatially extensive (Mock et al., 2008). This prediction is consistent with findings from ground-based analyses of aspen stem mortality

(Blonder et al., 2021). However, regeneration and species interactions may lead to more complex and less predictable outcomes (Marchetti et al., 2011; Rogers et al., 2014), e.g., as in aspen forests affected by fungal cankers and drought (Ruess et al., 2021) as well as insect pathogens (Crouch et al., 2021).

4.5 | Outlook

The success of the aspen cytotype classification suggests that further upscaling is possible in aspen or other species. Orbital imaging spectrometers can provide similar spectral data at coarser resolutions, and orbital multiband imagers (Sentinel-2, Landsat 8) capture coarser estimates of relevant spectral ranges. With decreased spatial resolution, future upscaled models will need to account for nonlinear spectral mixing in tree canopies. Remote sensing of cytotype in other species besides aspen also should be possible. The likelihood is highest if the imagery is available at high enough resolution to obtain spectrally pure pixels, or endmembers are available to unmix pixels.

There is also a large role for allelic genetic variation in determining fitness in aspen (e.g., Blonder et al., 2021; Einspahr et al., 1963; Kanaga et al., 2008; Lindroth & Clair, 2013). We did not focus on such effects in this study because we anticipated cytotype mapping would be a relatively straightforward machine learning problem (low number of classes, spectral separability clearly present in data). It also may become possible to map other genetic features using more advanced spectral data and machine learning algorithms. Some genes that have strong one-to-one mappings to phenotypes associated with spectral variation may be detectable from imagery, as could other features (e.g., sex, heterozygosity, or gene diversity). On the contrary, it is likely that many allelic genetic features will have no phenotypic impacts that cause variation in spectral properties, and will, therefore, remain out of reach for remote sensing approaches.

In conclusion, maps of cytotype variation provide a novel resource for land management, in helping map potential population responses to climate change or management. Genetic maps soon could be incorporated into restoration tools (Brabec et al., 2017; Richardson & Chaney, 2018). Thus, there is great potential for further integration of ecological genomics and remote sensing (Bush et al., 2017; Fitzpatrick & Keller, 2015).

ACKNOWLEDGMENTS

Janet Franklin, Bryce Richardson, and several anonymous reviewers provided feedback on the manuscript. Carol A. Rowe provided key assistance with DNA sequence assembly and analysis. Gavin Belfry, Marco Castaneda, Nallely Centeno, Lake Crawford, Tristram Dodge, Pierre Gaüzère, Jake Gerber, Lars Iversen, Thomas Jenkins, Deidra Johnson, Jocelyn Navarro, Carol Rosas, G. Richard Strimbeck, Susan Toepfer, Savannah Troy, Connie Webb, Aidan Wells, and JaHyun Yang provided field assistance. M. Otis Clyne, Deidra Johnson, Madison Lusk, Crystal Suazo, Noah Weakly, and Brigitte Jaramillo assisted with laboratory and spatial analyses. Jim Childers and Osvaldo Sala lent laboratory equipment. Bill Anderegg, Choy Huang, Shannon Sprott, and Ken Williams assisted with site selection. Rozália Kapás, Kenny Helsen, and Jolanta Rieksta led preliminary analyses that enabled this project. Jennie Reithel and the Rocky Mountain Biological Laboratory assisted with USFS permitting. Data used in this research were obtained through the NEON Assignable Assets program by the Department of Energy's Watershed Function Scientific Focus Area. Student participation was supported by the National Science Foundation Research Experience for Undergraduates (NSF-REU) program under grant DBI-1755522 and the Western Alliance to Expand Student Opportunities, in part by a cooperative agreement with NSF and the Hispanic Research Center at Arizona State University. Machine learning was supported by Microsoft's AI 4 Earth program. BB was supported by Arizona State University's School of Life Sciences. KM was supported by UAES project 1291, and this manuscript is UAES paper #9439. KDC was supported by the National Science Foundation under an NSF EAR Postdoctoral Fellowship Grant Number: 1725788. PGB was supported by the Jet Propulsion Laboratory, California Institute of Technology, under a contract with the National Aeronautics and Space Administration, and acknowledges support from the US government.

AUTHOR CONTRIBUTIONS

Benjamin Blonder conceived the study and led statistical analyses and writing. Benjamin Blonder and Courtenay A. Ray and K. Dana Chadwick collected field data. James A. Walton and Karen E. Mock carried out genetic analyses. Philip G. Brodrick and K. Dana Chadwick carried out remote sensing and machine learning analyses of hyperspectral and LiDAR data. Ian K. Breckheimer carried out remote sensing analyses of LiDAR data. Suzanne Marchetti provided guidance on fieldwork and contributed to writing.

CONFLICT OF INTEREST

The authors have no conflict of interest to declare.

DATA AVAILABILITY STATEMENT

Reflectance and canopy height data, shade masks, trait maps, and code are available on DOE's ESS-DIVE (Brodrick et al., 2020; Chadwick, Brodrick, Grant, Henderson, et al., 2020; Goulden et al., 2020). DNA sequence data and ground-truth cytotype data are available via (Blonder, Walton, et al., 2020). Aspen landcover maps, cytotype maps, and code are available on DOE's ESS-DIVE (Brodrick et al., 2021). Statistical analysis code and instructions for replicating all analyses are archived in Blonder (2022) and updated at https://github.com/bblonder/aspen_neon. All spatial datasets are also available for visualization and reuse in Google Earth Engine at https://code.earthengine.google.com/136b471efd6c5ba78b99596fc140e44b.

ORCID

Benjamin Blonder https://orcid.org/0000-0002-5061-2385
Philip G. Brodrick https://orcid.org/0000-0001-9497-7661
James A. Walton https://orcid.org/0000-0003-3211-5083
Katherine Dana Chadwick https://orcid.org/0000-0002-5633-4865

Ian K. Breckheimer https://orcid.org/0000-0002-4698-977X
Courtenay A. Ray https://orcid.org/0000-0002-2276-5915
Karen E. Mock https://orcid.org/0000-0002-8357-4434

REFERENCES

Adams, H. D., Zeppel, M. J., Anderegg, W. R., Hartmann, H., Landhäusser, S. M., Tissue, D. T., Huxman, T. E., Hudson, P. J., Franz, T. E., Allen, C. D., & Anderegg, L. D. (2017). A multi-species synthesis of physiological mechanisms in drought-induced tree mortality. *Nature Ecology & Evolution*, *1*, 1285–1291.

Anderegg, W. R. L., Flint, A., Huang, C.-Y., Flint, L., Berry, J. A., Davis, F. W., Sperry, J. S., & Field, C. B. (2015). Tree mortality predicted from drought-induced vascular damage. *Nature Geoscience*, *8*, 367–371. https://doi.org/10.1038/ngeo2400

Anderegg, W. R., Plavcová, L., Anderegg, L. D., Hacke, U. G., Berry, J. A., & Field, C. B. (2013). Drought's legacy: Multiyear hydraulic deterioration underlies widespread aspen forest die-off and portends increased future risk. *Global Change Biology*, *19*, 1188–1196. https://doi.org/10.1111/gcb.12100

Asner, G. P. (1998). Biophysical and biochemical sources of variability in canopy reflectance. *Remote Sensing of Environment*, *64*, 234–253. https://doi.org/10.1016/S0034-4257(98)00014-5

Asner, G. P., Martin, R. E., Knapp, D. E., Tupayachi, R., Anderson, C. B., Sinca, F., Vaughn, N. R., & Llactayo, W. (2017). Airborne laser-guided imaging spectroscopy to map forest trait diversity and guide conservation. *Science*, *355*, 385–389. https://doi.org/10.1126/science.aaj1987

Baker, F. S. (1921). Two races of aspen. *Journal of Forestry*, *19*, 412–413.

Baldeck, C. A., Asner, G. P., Martin, R. E., Anderson, C. B., Knapp, D. E., Kellner, J. R., & Wright, S. J. (2015). Operational tree species mapping in a diverse tropical forest with airborne imaging spectroscopy. *PLoS One*, *10*, e0118403. https://doi.org/10.1371/journal.pone.0118403

Bell, D. M., Bradford, J. B., & Lauenroth, W. K. (2015). Scale dependence of disease impacts on quaking aspen (*Populus tremuloides*) mortality in the southwestern United States. *Ecology*, *96*, 1835–1845.

Benson, M. K., & Einspahr, D. W. (1967). Early growth of diploid, triploid and triploid hybrid aspen. *Forest Science*, *13*, 150–155.

Blonder, B. (2022). 1.0.0 bblonder/aspen_neon: Code supporting Blonder et al. 2022. https://doi.org/10.5281/zenodo.5800132

Blonder, B., Graae, B., Greer, B., Haagsma, M., Helsen, K., Kapas, R., Pai, H., Rieksta, J., Sapena, D., Still, C., & Strimbeck, G. R. (2020). Remote sensing of ploidy level in quaking aspen (*Populus tremuloides* Michx.). *Journal of Ecology*, *108*, 175–188.

Blonder, B., Ray, C., Walton, J., Castaneda, M., Chadwick, K. D., Clyne, M., Gaüzère, P., Iversen, L. L., Madison Lusk, G., Strimbeck, R., Troy, S., & Mock, K. E. (2021). Cytotype and genotype predict mortality and recruitment in Colorado quaking aspen (*Populus tremuloides*). *Ecological Applications*, *31*.

Blonder, B., Walton, J., & Mock, K. (2020). Ploidy and clonal membership in *Populus tremuloides* from RADseq data. https://doi.org/10.26078/jnpn-4a13

Brabec, M. M., Germino, M. J., & Richardson, B. A. (2017). Climate adaptation and post-fire restoration of a foundational perennial in cold desert: Insights from intraspecific variation in response to weather. *Journal of Applied Ecology*, *54*, 293–302.

Breckheimer, I. (2021). *A Composite High Resolution Canopy Height Map for the East River Watershed, Colorado*. Watershed Function SFA.

Brodrick, P. G., Anderegg, L. D. L., & Asner, G. P. (2019). Forest drought resistance at large geographic scales. *Geophysical Research Letters*, *46*, 2752–2760. https://doi.org/10.1029/2018GL081108

Brodrick, P., & Asner, G. (2017). Remotely sensed predictors of conifer tree mortality during severe drought. *Environmental Research Letters*, *12*, 115013. https://doi.org/10.1088/1748-9326/aa8f55

Brodrick, P. G., Chadwick, K. D., & Blonder, B. (2021). Aspen ploidy level and cover maps from NEON Airborne Observation Platform, 2018, Crested Butte, Colorado. EAGER SitS: Can remotely imaged vegetation characteristics provide a window into soil nutrient cycles?

Brodrick, P., Goulden, T., & Chadwick, D. (2020). Custom NEON AOP reflectance mosaics and maps of shade masks, canopy water content. *Watershed Function SFA*.

Bush, A., Sollmann, R., Wilting, A., Bohmann, K., Cole, B., Balzter, H., Martius, C., Zlinszky, A., Calvignac-Spencer, S., Cobbold, C. A., Dawson, T. P., Emerson, B. C., Ferrier, S., Gilbert, M. T. P., Herold, M., Jones, L., Leendertz, F. H., Matthews, L., Millington, J. D. A., … Yu, D. W. (2017). Connecting Earth observation to high-throughput biodiversity data. *Nature Ecology & Evolution*, *1*, 1–9. https://doi.org/10.1038/s41559-017-0176

Chadwick, K. D., & Asner, G. P. (2016). Organismic-scale remote sensing of canopy foliar traits in lowland tropical forests. *Remote Sensing*, *8*, 87. https://doi.org/10.3390/rs8020087

Chadwick, K. D., & Brodrick, P. G. (2020). pgbrodrick/acorn_atmospheric_correction: v1.0.0 (Version v1.0.0). https://doi.org/10.5281/zenodo.3955363

Chadwick, K. D., Brodrick, P. G., Grant, K., Goulden, T., Henderson, A., Falco, N., Wainwright, H., Williams, K. H., Bill, M., Breckheimer, I., Brodie, E. L., Steltzer, H., Williams, C. F. R., Blonder, B., Chen, J., Dafflon, B., Damerow, J., Hancher, M., Khurram, A., … Maher, K. (2020). Integrating airborne remote sensing and field campaigns for ecology and Earth system science. *Methods in Ecology and Evolution*, *11*, 1492–1508. https://doi.org/10.1111/2041-210X.13463

Chadwick, K. D., Brodrick, P. G., Grant, K., Henderson, A., Bill, M., Breckheimer, I., Williams, C. F. R., Goulden, T., Falco, N., McCormick, M., Musinsky, J., Pierce, S., Hastings Porro, M., Scott, A., Brodie, E., Hancher, M., Steltzer, H., Wainwright, H., Williams, K. & Maher, K. (2020). NEON AOP foliar trait maps, maps of model uncertainty estimates, and conifer map, East River, CO 2018.

Chadwick, K. D., Grant, K., Bill, M., Henderson, A., Scott, A., & Maher, K. (2020). Site-level Foliar C, N, delta^{13}C data from samples collected during field survey associated with NEON AOP survey, East River, CO 2018. https://doi.org/10.15485/1631278

Clark, M. L., Roberts, D. A., & Clark, D. B. (2005). Hyperspectral discrimination of tropical rain forest tree species at leaf to crown scales. *Remote Sensing of Environment*, *96*, 375–398. https://doi.org/10.1016/j.rse.2005.03.009

Coleman, T. W., Graves, A. D., Heath, Z., Flowers, R. W., Hanavan, R. P., Cluck, D. R., & Ryerson, D. (2018). Accuracy of aerial detection surveys for mapping insect and disease disturbances in the United States. *Forest Ecology and Management*, *430*, 321–336. https://doi.org/10.1016/j.foreco.2018.08.020

Crouch, C. D., Grady, A. M., Wilhelmi, N. P., Hofstetter, R. W., DePinte, D. E., & Waring, K. M. (2021). Oystershell scale: An emerging invasive threat to aspen in the southwestern US. *Biological Invasions*, *23*(9), 2893–2912. https://doi.org/10.1007/s10530-021-02545-0

Curran, P. J. (1989). Remote sensing of foliar chemistry. *Remote Sensing of Environment*, *30*, 271–278. https://doi.org/10.1016/0034-4257(89)90069-2

Czyż, E. A., Guillén Escribà, C., Wulf, H., Tedder, A., Schuman, M. C., Schneider, F. D., & Schaepman, M. E. (2020). Intraspecific genetic variation of a *Fagus sylvatica* population in a temperate forest derived from airborne imaging spectroscopy time series. *Ecology and Evolution*, *10*, 7419–7430.

DeByle, N. V., & Winokur, R. P. (1985). Aspen: Ecology and management in the western United States. *USDA Forest Service General Technical Report RM-119. Rocky Mountain Forest and Range Experiment Station, Fort Collins, Colo.*, 119.

DeWoody, J., Rowe, C. A., Hipkins, V. D., & Mock, K. E. (2008). "Pando" lives: Molecular genetic evidence of a giant aspen clone in central

Utah. *Western North American Naturalist*, *68*, 493–497. https://doi.org/10.3398/1527-0904-68.4.493

Díaz, S., Kattge, J., Cornelissen, J. H. C., Wright, I. J., Lavorel, S., Dray, S., Reu, B., Kleyer, M., Wirth, C., Colin Prentice, I., Garnier, E., Bönisch, G., Westoby, M., Poorter, H., Reich, P. B., Moles, A. T., Dickie, J., Gillison, A. N., Zanne, A. E., … Gorné, L. D. (2016). The global spectrum of plant form and function. *Nature*, *529*(7585), 167–171. https://doi.org/10.1038/nature16489

Dixon, G. B., & DeWald, L. E. (2015). Microsatellite survey reveals possible link between triploidy and mortality of quaking aspen in Kaibab National Forest, Arizona. *Canadian Journal of Forest Research*, *45*, 1369–1375. https://doi.org/10.1139/cjfr-2014-0566

Donaldson, J. R., Stevens, M. T., Barnhill, H. R., & Lindroth, R. L. (2006). Age-related shifts in leaf chemistry of clonal aspen (*Populus tremuloides*). *Journal of Chemical Ecology*, *32*, 1415–1429. https://doi.org/10.1007/s10886-006-9059-2

Einspahr, D. W., Van Buijtenen, J., & Peckham, J. (1963). Natural variation and heritability in triploid aspen. *Silvae Genetica*, *12*, 51–58.

Elith, J., & Leathwick, J. R. (2009). Species distribution models: Ecological explanation and prediction across space and time. *Annual Review of Ecology Evolution and Systematics*, *40*, 677–697. https://doi.org/10.1146/annurev.ecolsys.110308.120159

Every, A. D., & Wiens, D. (1971). Triploidy in Utah aspen. *Madroño*, *21*, 138–147.

Ferreira, M. P., Zortea, M., Zanotta, D. C., Shimabukuro, Y. E., & de Souza Filho, C. R. (2016). Mapping tree species in tropical seasonal semi-deciduous forests with hyperspectral and multispectral data. *Remote Sensing of Environment*, *179*, 66–78. https://doi.org/10.1016/j.rse.2016.03.021

Fitzpatrick, M. C., & Keller, S. R. (2015). Ecological genomics meets community-level modelling of biodiversity: Mapping the genomic landscape of current and future environmental adaptation. *Ecology Letters*, *18*, 1–16. https://doi.org/10.1111/ele.12376

Flansburg, A. L. (2018). *Trembling aspen triploid advantage has a physiological basis with geographic caveats*. University of Wisconsin.

Fricker, G. A., Ventura, J. D., Wolf, J. A., North, M. P., Davis, F. W., & Franklin, J. (2019). A convolutional neural network classifier identifies tree species in mixed-conifer forest from hyperspectral imagery. *Remote Sensing*, *11*, 2326. https://doi.org/10.3390/rs11192326

Gompert, Z., Lucas, L. K., Nice, C. C., Fordyce, J. A., Forister, M. L., & Buerkle, C. A. (2012). Genomic regions with a history of divergent selection affect fitness of hybrids between two butterfly species. *Evolution*, *66*, 2167–2181. https://doi.org/10.1111/j.1558-5646.2012.01587.x

Gompert, Z., Mock, K. E. (2017). Detection of individual ploidy levels with genotyping-by-sequencing (GBS) analysis. *Molecular Ecology Resources*, *17*, 1156–1167. https://doi.org/10.1111/1755-0998.12657

Goulden, M. L., & Bales, R. C. (2019). California forest die-off linked to multi-year deep soil drying in 2012–2015 drought. *Nature Geoscience*, *12*, 632–637. https://doi.org/10.1038/s41561-019-0388-5

Goulden, T., Hass, B., Brodie, E., Chadwick, K. D., Falco, N., Maher, K., & Wainwright, H. (2020). *NEON AOP survey of upper east river CO watersheds: LAZ files, LiDAR surface elevation, terrain elevation, and canopy height rasters*. ESS-DIVE.

Goulden, T., & Musinsky, J. (2020). *Post survey report for AOP assignable asset collection of crested butte, CO*. ESS-DIVE.

Greer, B. T., Still, C., Cullinan, G. L., Brooks, J. R., & Meinzer, F. C. (2017). Polyploidy influences plant–environment interactions in quaking aspen (*Populus tremuloides* Michx.). *Tree Physiology*, 1–11.

Heidemann, H. K. (2018). Lidar base specification. *US Geological Survey*.

Kanaga, M. K., Ryel, R. J., Mock, K. E., & Pfrender, M. E. (2008). Quantitative-genetic variation in morphological and physiological traits within a quaking aspen (*Populus tremuloides*) population. *Canadian Journal of Forest Research*, *38*, 1690–1694.

Kay, C. E. (2000). Native burning in western North America: implications for hardwood forest management. In *Yaussy, Daniel A., comp. 2000. Proceedings: workshop on fire, people, and the central hardwoods landscape; 2000 March 12-14; Richmond, KY. Gen. Tech. Rep. NE-274. Newtown Square, PA: US Department of Agriculture, Forest Service, Northeastern Research Station: 19-27.*

Keeler, K. H. (1998). Population biology of intraspecific polyploidy in grasses. In G. P. Cheplick (Ed.), *Population biology of grasses* (pp. 183–206). Cambridge University Press.

Khosravipour, A., Skidmore, A. K., Isenburg, M., Wang, T., & Hussin, Y. A. (2014). Generating pit-free canopy height models from airborne Lidar. *Photogrammetric Engineering & Remote Sensing*, *80*, 863–872. https://doi.org/10.14358/PERS.80.9.863

Kruger, E. L., Keefover-Ring, K., Holeski, L. M., & Lindroth, R. L. (2020). To compete or defend: Linking functional trait variation with life-history tradeoffs in a foundation tree species. *Oecologia*, *192*(4), 893–907. https://doi.org/10.1007/s00442-020-04622-y

Laport, R. G., Minckley, R. L., & Ramsey, J. (2012). Phylogeny and cytogeography of the North American creosote bush (*Larrea tridentata*, Zygophyllaceae). *Systematic Botany*, *37*, 153–164.

Levin, D. A. (1983). Polyploidy and novelty in flowering plants. *The American Naturalist*, *122*, 1–25. https://doi.org/10.1086/284115

Lindroth, R. L., & Clair, S. B. S. (2013). Adaptations of quaking aspen (*Populus tremuloides* Michx.) for defense against herbivores. *Forest Ecology and Management*, *299*, 14–21. https://doi.org/10.1016/j.foreco.2012.11.018

Little, D. L. (1971). Atlas of United States trees vol. 1, in: Miscellaneous publication 1146. United States Department of Agriculture, Forest Service.

Liu, X., & Biondi, F. (2021). Inter-specific transpiration differences between aspen, spruce, and pine in a sky-island ecosystem of the North American Great Basin. *Forest Ecology and Management*, *491*, 119157. https://doi.org/10.1016/j.foreco.2021.119157

Madritch, M. D., Kingdon, C. C., Singh, A., Mock, K. E., Lindroth, R. L., & Townsend, P. A. (2014). Imaging spectroscopy links aspen genotype with below-ground processes at landscape scales. *Philosophical Transactions of the Royal Society of London B: Biological Sciences*, *369*, 20130194.

Marchetti, S. B., Worrall, J. J., & Eager, T. (2011). Secondary insects and diseases contribute to sudden aspen decline in southwestern Colorado, USA. *Canadian Journal of Forest Research*, *41*, 2315–2325. https://doi.org/10.1139/x11-106

Martin, R. E., Chadwick, K. D., Brodrick, P. G., Carranza-Jimenez, L., Vaughn, N. R., & Asner, G. P. (2018). An approach for foliar trait retrieval from airborne imaging spectroscopy of tropical forests. *Remote Sensing*, *10*, 199. https://doi.org/10.3390/rs10020199

Martinez-Vilalta, J., Anderegg, W. R., Sapes, G., & Sala, A. (2019). Greater focus on water pools may improve our ability to understand and anticipate drought-induced mortality in plants. *New Phytologist*, *223*, 22–32. https://doi.org/10.1111/nph.15644

Mitton, J. B., & Grant, M. C. (1996). Genetic Variation and the Natural History of Quaking Aspen: The ways in which aspen reproduces underlie its great geographic range, high levels of genetic variability, and persistence. *BioScience*, *46*, 25–31. https://doi.org/10.2307/1312652

Mock, K. E., Callahan, C. M., Islam-Faridi, M. N., Shaw, J. D., Rai, H. S., Sanderson, S. C., Rowe, C. A., Ryel, R. J., Madritch, M. D., Gardner, R. S., & Wolf, P. G. (2012). Widespread triploidy in western North American aspen (*Populus tremuloides*). *PLoS One*, *7*, e48406. https://doi.org/10.1371/journal.pone.0048406

Mock, K. E., Rowe, C., Hooten, M. B., Dewoody, J., & Hipkins, V. (2008). Clonal dynamics in western North American aspen (*Populus tremuloides*). *Molecular Ecology*, *17*, 4827–4844.

Morgan, M. D. (1969). Ecology of aspen in Gunnison County, Colorado. *American Midland Naturalist*, 204–228. https://doi.org/10.2307/2423831

NOAA. (2019). Gridded Annual US Drought Monitor (USDM) Maps. https://www.drought.gov/drought/data-gallery/gridded-annual-us-drought-monitor-usdm-maps

Parmesan, C., & Yohe, G. (2003). A globally coherent fingerprint of climate change impacts across natural systems. *Nature*, *421*, 37–42. https://doi.org/10.1038/nature01286

Petit, C., Bretagnolle, F., & Felber, F. (1999). Evolutionary consequences of diploid–polyploid hybrid zones in wild species. *Trends in Ecology & Evolution*, *14*, 306–311. https://doi.org/10.1016/S0169-5347(99)01608-0

Richardson, B. A., & Chaney, L. (2018). Climate-based seed transfer of a widespread shrub: Population shifts, restoration strategies, and the trailing edge. *Ecological Applications*, *28*, 2165–2174. https://doi.org/10.1002/eap.1804

Roddy, A. B., Théroux-Rancourt, G., Abbo, T., Benedetti, J. W., Brodersen, C. R., Castro, M., Castro, S., Gilbride, A. B., Jensen, B., Jiang, G.-F., Perkins, J. A., Perkins, S. D., Loureiro, J., Syed, Z., Thompson, R. A., Kuebbing, S. E., & Simonin, K. A. (2020). The scaling of genome size and cell size limits maximum rates of photosynthesis with implications for ecological strategies. *International Journal of Plant Sciences*, *181*, 75–87. https://doi.org/10.1086/706186

Rogers, P. C., Landhäusser, S. M., Pinno, B. D., & Ryel, R. J. (2014). A functional framework for improved management of western North American aspen (*Populus tremuloides* Michx.). *Forest Science*, *60*, 345–359. https://doi.org/10.5849/forsci.12-156

Rowe, C. (2019). vcf2Jaccard. https://github.com/carol-rowe666/vcf2Jaccard

Ruess, R. W., Winton, L. M., & Adams, G. C. (2021). Widespread mortality of trembling aspen (*Populus tremuloides*) throughout interior Alaskan boreal forests resulting from a novel canker disease. *PLoS One*, *16*, e0250078. https://doi.org/10.1371/journal.pone.0250078

Singh, A., Serbin, S. P., McNeil, B. E., Kingdon, C. C., & Townsend, P. A. (2015). Imaging spectroscopy algorithms for mapping canopy foliar chemical and morphological traits and their uncertainties. *Ecological Applications*, *25*, 2180–2197. https://doi.org/10.1890/14-2098.1

Sperry, J. S., Meinzer, F. C., & McCULLOH, K. A. (2008). Safety and efficiency conflicts in hydraulic architecture: Scaling from tissues to trees. *Plant, Cell & Environment*, *31*, 632–645. https://doi.org/10.1111/j.1365-3040.2007.01765.x

Stasinski, L., White, D. M., Nelson, P. R., Ree, R. H., & Meireles, J. E. (2021). Reading light: Leaf spectra capture fine-scale diversity of closely related, hybridizing arctic shrubs. *New Phytologist*, *232*(6), 2283–2294. https://doi.org/10.1111/nph.17731

Stebbins, G. L. (1971). Chromosomal evolution in higher plants. *Chromosomal evolution in higher plants*.

Tai, X., Mackay, D. S., Anderegg, W. R. L., Sperry, J. S., & Brooks, P. D. (2017). Plant hydraulics improves and topography mediates prediction of aspen mortality in southwestern USA. *New Phytologist*, *213*, 113–127.

Théroux-Rancourt, G., Roddy, A. B., Earles, J. M., Gilbert, M. E., Zwieniecki, M. A., Boyce, C. K., Tholen, D., McElrone, A. J., Simonin, K. A., & Brodersen, C. A. (2021). Maximum CO_2 diffusion inside leaves is limited by the scaling of cell size and genome size. *Proceedings of the Royal Society B*, *288*, 20203145.

Tran, H., Zhang, J., Cohard, J.-M., Condon, L. E., & Maxwell, R. M. (2020). Simulating groundwater-streamflow connections in the Upper Colorado River Basin. *Groundwater*, *58*, 392–405. https://doi.org/10.1111/gwat.13000

Trugman, A. T., Detto, M., Bartlett, M. K., Medvigy, D., Anderegg, W. R. L., Schwalm, C., Schaffer, B., & Pacala, S. W. (2018). Tree carbon allocation explains forest drought-kill and recovery patterns. *Ecology Letters*, *21*, 1552–1560. https://doi.org/10.1111/ele.13136

Wainwright, H., & Williams, K. (2017). LiDAR collection in August 2015 over the East River Watershed, Colorado, USA.

Worrall, J. J., Egeland, L., Eager, T., Mask, R. A., Johnson, E. W., Kemp, P. A., & Shepperd, W. D. (2008). Rapid mortality of *Populus tremuloides* in southwestern Colorado, USA. *Forest Ecology and Management*, *255*, 686–696. https://doi.org/10.1016/j.foreco.2007.09.071

Worrall, J. J., Rehfeldt, G. E., Hamann, A., Hogg, E. H., Marchetti, S. B., Michaelian, M., & Gray, L. K. (2013). Recent declines of *Populus tremuloides* in North America linked to climate. *Forest Ecology and Management*, *299*, 35–51. https://doi.org/10.1016/j.foreco.2012.12.033

Youngentob, K. N., Zdenek, C., & van Gorsel, E. (2016). A simple and effective method to collect leaves and seeds from tall trees. *Methods in Ecology and Evolution*, *7*, 1119–1123. https://doi.org/10.1111/2041-210X.12554

SUPPORTING INFORMATION

Additional supporting information may be found in the online version of the article at the publisher's website.

How to cite this article: Blonder, B., Brodrick, P. G., Walton, J. A., Chadwick, K. D., Breckheimer, I. K., Marchetti, S., Ray, C. A., & Mock, K. E. (2021). Remote sensing of cytotype and its consequences for canopy damage in quaking aspen. *Global Change Biology*, 00, 1–14. https://doi.org/10.1111/gcb.16064